Finite Element Based Transient Heat Transfer Analysis of Ti2AlNb Electron Beam Welds Using Hybrid Volumetric Heat Source

Sohini Chowdhury[1], Yadaiah Nirsanametla[2*] and Manapuram Muralidhar[3]
Department of Mechanical Engineering, North Eastern Regional Institute of Science and Technology, Nirjuli 791109, Arunachal Pradesh, India
E-mail: [1]sohinidme@gmail.com, [2]ny@nerist.ac.in, [3]mm@nerist.ac.in

DOI : 10.22486/iwj/2019/v52/i1/178190

ABSTRACT

Titanium based alloy Ti2AlNb is considered as a formidable structural material for advanced aero-engine applications due to its low density and high melting point temperature. Moreover, titanium based Ti2AlNb alloy is reactive towards atmospheric elements at an elevated temperature and hence conventional welding techniques do not fit to weld this type of materials. Furthermore, electron beam (EB) welding process is preferable to join Ti2AlNb alloy as it provides vacuum environment and possess high energy density with relatively minimum thermal input. EB welding produces deep and narrow penetration welds which leads to minimum weld induced stresses and distortion. In the recent past, several experimental analysis have been presented to comprehend the weld pool geometry during fusion welding procedures. Moreover, the phenomenological occurrence within and vicinity of the molten weld zone are primary focus of analysis. Therefore, a three-dimensional (3D) numerical model is paramount to interpret the physical occurrence of welding operation using a suitable volumetric heat source model. Nevertheless, in the current investigation, a transient heat transfer model based on finite element (FE) method is developed to simulate electron beam welds of titanium based Ti2AlNb alloy. In the course of modeling, a suitable thermal model is selected based on weldment profile and is quite accountable for determining accuracy of heat transfer analysis. The authors have considered a composite heat source model, comprising of two dimensional Gaussian distributed double ellipsoidal heat source at the top section and volumetric conical heat source through thickness of the cross section. Along with composite heat source model; material properties and latent heat of fusion as a function of temperature have been incorporated during modeling. The developed numerical heat transfer process model predicts the time-temperature history, cooling rates, weld bead dimensions and shapes. To verify the effectiveness of developed process model, the computed results are evaluated with experimentally estimated weld bead dimensions and profile. The numerical results indicated that the weld geometry characteristics and thermal history are in good accordance with the experimental data with less than 6% error. Moreover, the computed FE model results lays foundation for the estimation of welding induced distortion and residual stresses further.

Keywords: Ti2AlNb alloy; electron beam welding; FEM; thermal analysis; composite heat source.

1.0 INTRODUCTION

High power density electron beam allows welding a wide scope of geometries with an equally wider span of thicknesses for applications where narrow heat affected zone (HAZ) and high aspect ratio are indispensable. Owing to very high specific energy of electron beam, the material undergoes intense vaporization in vacuum atmosphere resulting in the evolution of a deep vapour cavity, referred to as 'key hole' surrounded by molten metal. Moreover, electron beam welding (EBW) operation possesses superior characteristics like minimum thermal input and high power density. This results into minimal weld induced stresses and strains, making EBW superior over other welding techniques. Furthermore, it has extensive applications in industries due to indigenous features and flexibility towards joint preparation [1-2].

Titanium based Ti2AlNb alloy acquire desirable combination of attributes such as high strength, low density, corrosion resistance and excellent processability. On account of these remarkable attributes, titanium and its alloy welds are best suited for aerospace applications. Several experimental investigations have been carried out earlier examine weldability and mechanical characteristics of Ti2AlNb alloy using laser beam and other traditional welding processes[3-7]. However, welded joints produced by laser and friction welding techniques displayed high hardness and low ductility values at an elevated temperature due to evolution of O phase precipitation at the grain boundary. Using EBW process, joints exhibited improved mechanical properties and refined grain size at the boundary. Therefore, EBW is considered to be a favorable joining technique to weld titanium and its alloys. Tan et al. [8-9] welded Ti2AlNb and TC11 with EBW process to examine the microstructure property and mechanical characteristics. The dissimilar electron beam weldment of Ti2AlNb and TC11displayedenhancedtensile strength and impact toughness along with refined grains at fusion zone. Li et al. [10] reported the effect of EBW process variables on weld shape of Ti2AlNb alloy and welding induced distortions. They pointed out that variation in focus current has significant impact on weld shape and deformation of the workpiece.

Numerical modeling is considered to be an efficient tool for design and production of fabricated parts with suitable process variables. Compared to experimental analysis, numerical process modeling provides significant detailed information such as weld bead shape and dimensions, thermal cycles, cooling rates, welding induced residual stresses and distortion for a given set of process parameters [11-15]. In the past few decades, several researchers performed heat transfer and stress analysis to understand the physics of weld pool formation and stresses induced after welding [16-18]. Luo et al. [16] established a combined heat source model comprising of Gaussian distributed surface heat flux and conical power density distribution to reproduce the thermal effect at surface and in keyhole on account of vaporization of metal elements in AZ61 magnesium alloying elements. To account the variation in keyhole shape due to focus current alteration, the authors adjusted the coefficient of power in combined thermal source model. Chiumenti et al. [17] developed an ad-hoc heat source to reproduce the actual power distribution at the surface and absorption in keyhole through numerical simulation procedure.

Also, Lacki et al. [18] carried out thermo-mechanical analysis of electron beam welded tubes based on conical heat source model with uniform power distribution. The authors pointed out that the magnitude of welding induced stresses is dependent on material yield stress at a specified temperature. Lacki et al. [19] developed a partial least square-finite element model (PLS-FEM) to estimate the fusion zone shape and distribution of residual stresses in chrome-nickel alloy plates. Bardel et al. [20] presented a thermo-metallurgical approach; whereby the thermal model reproduced the configuration of the fusion zone and determined thermal history based on equivalent Gaussian distributed truncated heat source model. They established thermal and microstructural model to compute the proportion of distinct phases in the welded specimen which was later implemented to FE software to measure the residual stresses. From the esteemed literature, it is identified that an appropriate thermal source model increases the accuracy of the developed process model. Moreover, numerical modeling of EBW process utilizing volumetric heat source models is not explored well. Therefore, in the present work, authors have developed a thermal model using combined heat source model comprising of two dimensional Gaussian distributed double ellipsoidal power density distribution and three dimensional Gaussian distributed conical power density distribution to estimate thermal behavior and weld bead dimensions.

2.0 THEORETICAL BACKGROUND

The thermal analysis is modelled by solving the conservation of energy equation in three dimension (3D). For fusion welding processes, 3D governing heat conduction equation with thermal source moving along γ–axis is represented mathematically as

$$\lambda\left(\frac{\partial^2 T}{\partial x^2}+\frac{\partial^2 T}{\partial y^2}+\frac{\partial^2 T}{\partial z^2}\right)+\dot{q}=\rho C\left(\frac{\partial T}{\partial t}-v\frac{\partial T}{\partial y}\right) \quad \text{.... (1)}$$

where λ, T, $\dot{q}$, ρ, C and ν represent thermal conductivity in W m^{-1} K^{-1}, temperature in K^{-1}, heat source per unit volume in Wm^{-3}, density in kgm^{-3}, specific heat capacity in J $K^{-1}$and velocity of the heat source in ms^{-1} respectively. However, heat loss due to convection is neglected in EBW operation since, it is operated in a vacuum chamber. Therefore, heat dissipation through radiation is only taken into account from the material surface as high thermal field is induced in the welded zone during the welding process. **Fig. 1** represents a schematic of transverse cross section of solution domain along with boundary conditions. The keyhole energy is balanced amongst beam heat flux, conduction and radiation heat transfer. The energy balance equation can be mathematically expressed as:

$$\lambda\left(\frac{\partial T}{\partial n}\right)+q_{ebw}+\sigma\varepsilon(T^4-T_\infty^4)=0 \quad \text{.... (2)}$$

where η represent cross sectional surface of the specimen, q_{ebw} represent input thermal flux at the surface of the specimen. σ, ε and T∞ represent Stephen Boltzman constant, radiation heat transfer coefficient and temperature at ambient atmosphere.

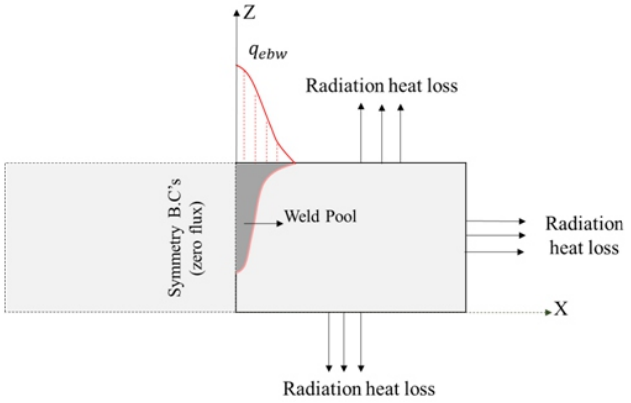

Fig. 1 : Schematic of solution domain along with boundary condition.

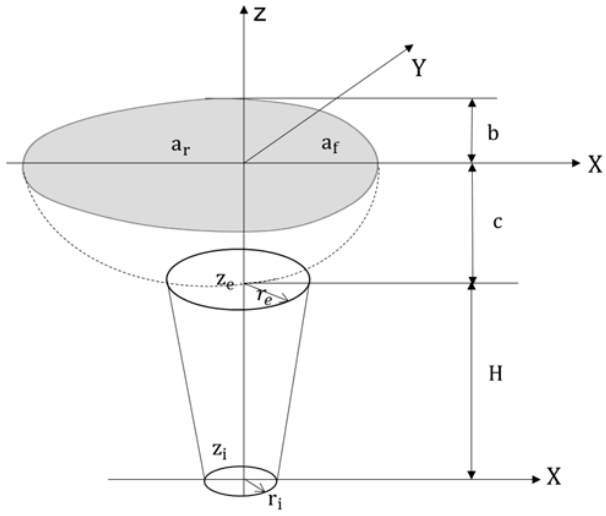

Fig. 2 : Representation of combined heat source model

An initial condition has to be defined at time, t=0, since simulation process is transient in nature and it is mathematically represented as

$$T(x, y, z, O) = T\infty \quad \text{.... (3)}$$

where T∞ is ambient temperature.

A combined thermal model comprising of double ellipsoidal distribution and conical body heat source distribution is used in the present work. In this model, Gaussian distributed double ellipsoid is considered on top surface of the plate while three dimensional conical body heat source distribution is incorporated through the thickness of the plate. **Fig. 2** illustrates the schematic of composite heat source model. The mathematical representation of double ellipsoidal power density distribution is

$$\dot{q}_f(x,y)=\frac{12\sqrt{3}Qf_f}{\pi\sqrt{\pi}b(a_r+a_f)}exp\left(-\frac{3x^2}{a_f^2}-\frac{3y^2}{b^2}\right) \quad \text{.... (4)}$$

$$\dot{q}_r(x,y)=\frac{12\sqrt{3}Qf_r}{\pi\sqrt{\pi}b(a_r+a_f)}exp\left(-\frac{3x^2}{a_r^2}-\frac{3y^2}{b^2}\right) \quad \text{.... (5)}$$

while the conical heat source power density distribution can be represented mathematically as follows

$$\dot{q}_{con}(r,z)=\frac{9Qfe^3}{\pi Il(e^3-1)(r_e^2+r_er_i+r_i^2)}exp(-3r^2/r_0^2) \quad c < z \le c + H) \text{ (6)}$$

$$r=\sqrt{(x-x_0-V_0t)^2+(y-y_0)^2} \quad O < z < H) \text{ (7)}$$

$$r_0(z)=r_e-(r_e-r_i)\frac{z_e-z}{z_e-z_i} \quad \text{..... (8)}$$

$$Q=\eta VI \quad \text{..... (9)}$$

where Q, η, V and I represent thermal energy absorbed by the specimen (W), thermal efficiency coefficient, accelerating voltage (kV), beam current intensity (A). f_f and f_r are the power distribution coefficients at the front and rear sections of double ellipsoidal thermal source distribution respectively. In addition, f represent power distribution coefficients of three dimensional conical thermal source. The total effective thermal flux in terms of power distribution fraction can be stated as:

$$f_f + f_r = 2 \quad \text{..... (10)}$$

Moreover, parameters of heat source model are mapped with experimentally estimated weld bead sizes.

3.0 RESULTS & DISCUSSION

In the present work, Ti2AlNb alloy of dimensions100 mm × 50 mm × 5 mm plate is considered to validate the developed process numerical model using composite heat source model. The substrate utilized in this investigation is Ti-22Al-25Nb sheet and the substrate is sectioned into 100 mm × 100 mm coupons from the sheet. A schematic of electron beam welding procedure is presented in **Fig. 3**. **Table 1** depicts the welding criterions considered in this work. However, the experimental results are adapted from an independent literature to verify the correctness of the developed process model [10]. Moreover, considering temperature dependent thermal properties in numerical modeling increases the accuracy and precision of computational results.

Thermal properties as a function of temperature such as density, thermal conductivity and specific heat are incorporated in the present work. In addition, temperature independent emissivity is implemented. Moreover, the thermal properties are extracted from independent literature [10-13]. **Fig.4** illustrates the temperature dependent thermal properties of Ti2AlNb alloy which is implemented during numerical simulations. Thermal conductivity (**Fig. 4(a)**) varies linearly till 1151.15K and then remains almost constant till 1781.15K with a 2% rise. However, it can be identified that there is a steep rise in thermal conductivity from 1872.95K till 2045.464K. The specific heat capacity (**Fig. 4 (b)**) behavior of Ti2AlNb alloy is linear with rise in temperature till 2010K. Moreover, density (**Fig. 4 (c)**) is determined to be constant with increase in temperature for the present analysis.

Table 1 : Electron beam welding criterions of Ti2AlNb alloy

Date Set No.	Accelerating Voltage (kV)	Beam Current (mA)	Focus Current (mA)	Weld Speed (mm/min)
1	60	25	2170	1000
2	60	25	2190	1000
3	60	25	2270	1000

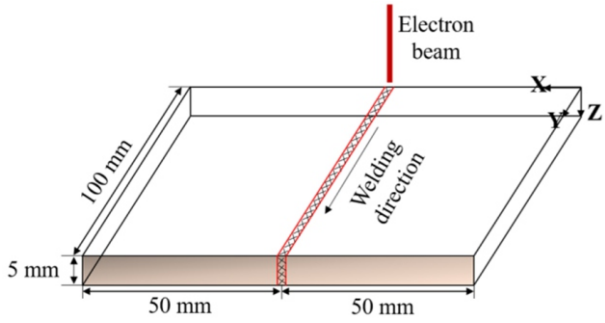

Fig. 3 : Electron beam welding process schematic representation.

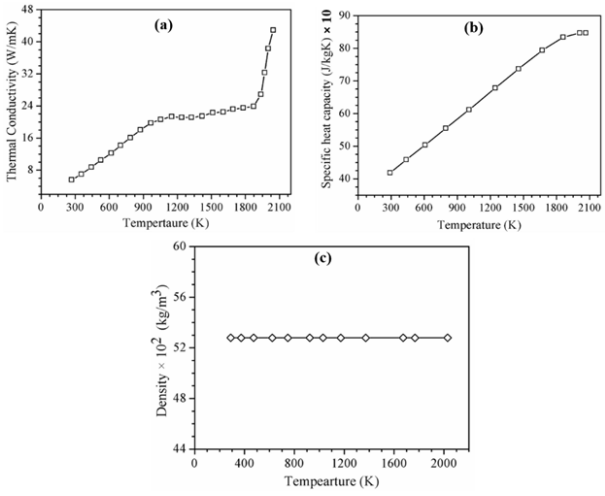

Fig. 4 : Thermal properties of material as a function of temperature (a) thermal conductivity, (b) specific heat and (c) density.

Estimated thermal behavior, weld bead dimensions and computational time substantially depends on mesh size and mesh type. Therefore, anon-uniform mesh is incorporated in the present work. This is implemented by defining are fined mesh at weld zone and gradually coarse mesh away from the weld zone. **Fig. 5** (**a, b** and **c**) shows the typical geometric model, non-uniform meshed solution domain and zoomed-in view of a section of FE model respectively. Since the heat source is symmetric in the transverse direction, only half section is considered for the analysis.

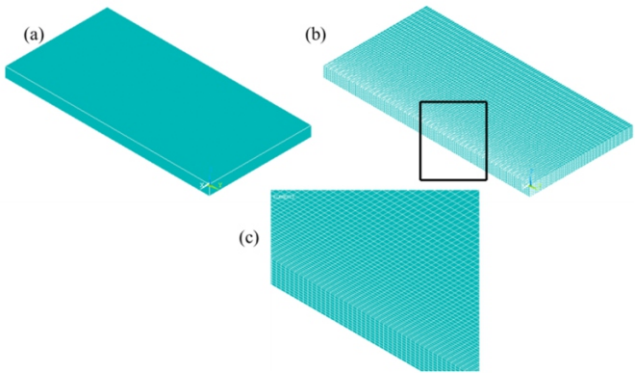

Fig. 5. : (a) Geometric model of dimensions 100 mm × 50 mm × 5 mm, (b) FE model with non-uniform mesh and (c) Zoomed-in view of part of FE model.

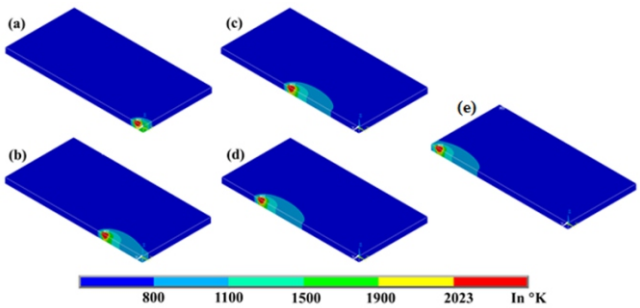

Fig. 6 : 3D transient isotherms for welding criterion #1 of Table 1 at time (a) 0.3 s, (b) 1.68 s, (c) 3 s, (d) 4.32 s and (e) 5.7 s.

Fig. 6 demonstrates 3D transient isotherms at five distinct positions for time, t = 0.3 s, 1.68 s, 3 s, 4.32 s and 5.7 s respectively for welding criterion #1 of **Table 1**. The red color region represents melt pool region having liquidus temperature of 2023 K. Moreover, the intercepts across X and Z – axes indicates half weld width and weld penetration. The comparison of fusion zone computed by FEM (left side) and cross section of Ti2AlNb alloy (right side) for welding criterion #1 of **Table 1** is illustrated in **Fig. 7**. Moreover, the calculated DOP and width are 3.4 mm and 2.44 mm corresponding to data set #1 of **Table 1**. The experimentally measured values of weld penetration and weld width for welding criterion #1 of **Table 1** are 3.5 mm and 2.26 mm. This reflects accuracy of the developed numerical process model by utilizing a composite heat source model for EBW process.

An overall computable comparison of estimated and experimentally determined weld bead sizes is presented in **Fig. 8** for welding criterions of **Table 1**. The % error between computed and experimentally determined weld bead sizes is within an acceptable limit (6). It is easily identified from **Fig. 8 (a)** that weld width reduces as focus current changes from 2170 mA to 2190 mA. However, there is negligible rise in weld bead width as focus current is increased from 2190 mA to 2270 mA. The focus current has a remarkable influence on DOP as shown in **Fig. 8 (b)**. The depth of penetration has elevated from 3.4 mm to 5 mm as focus current is varied from 2170 mA to 2190 mA and with further increase in focus current the DOP was determined to be constant. Based on the measured and computed results, it is observed that a fair agreement has been achieved between experimental and numerical weld bead dimensions and shape for the corresponding welding criterion. This endorses the correctness of the developed numerical heat transfer process model using a composite heat source model for electron beam welding operation.

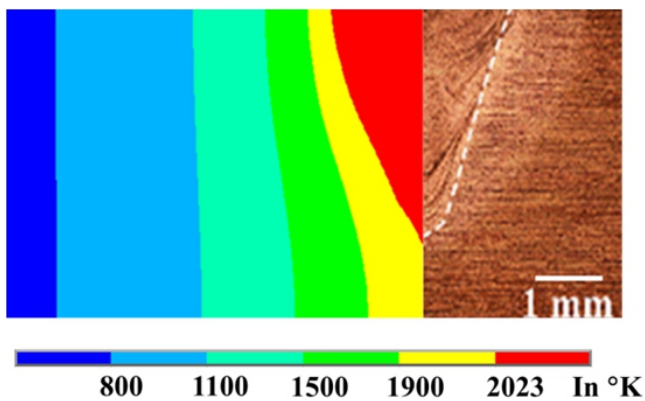

Fig. 7 : Comparison between computed transverse weld cross-section profile and corresponding experimentally measured weld macrograph for welding criterion #1 of Table 1.

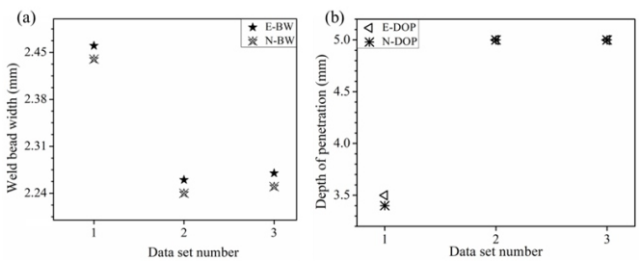

Fig. 8 : Overall quantitative comparison between experimental and computed (a) bead width and (b) weld penetration corresponding to process variables given in Table 1.

4.0 SUMMARY

A 3D FE based thermal process model was developed using composite thermal source model to inspect the thermal history and weld bead profiles of electron beam welded Ti2AlNb alloy specimen. From the present work, the conclusions are as follows:

(Ifocus current have a remarkable effect on weld penetration and have minimal impact on weld bead width during electron beam welding of Ti2AlNb alloy.

(ii) A numerical process model is developed using hybrid heat source model for EBW of Ti2AlNb alloy plates.

(iii) To verify the correctness of the developed process model, the computed weld bead dimensions and shapes were compared with experimentally measured values.

(iv) A sound agreement is achieved between experimental and simulated weld bead size and profile. The % error in computed and estimated weld dimension is > 6%.

ACKNOWLEDGEMENTS

The present paper is a revised version of an article presented in the International Congress (IC-2017) of the International Institute of Welding held in Chennai on December 07-09 2017 and organized by the Indian Institute of Welding.

The authors would like to thank Dr. Swarup Bag, Department of Mechanical Engineering, IIT Guwahati, Guwahati, India for his support during this work.

REFERENCES

[1] Rai R, Palmer TA, Elmer JW and Debroy T (2009); Heat transfer and fluid flow during electron beam welding of 304L stainless steel alloy, Weld. J., 8, pp. 54s-61s.

[2] Huang B, Chen X, Pang S and Hu R (2017); A three-dimensional model of coupling dynamics of keyhole and weld pool during electron beam welding, Int. J. Heat Mass Transf., 115, pp. 159-173.

[3] Chen X, Xie FQ, Ma TJ, Li WY and Wu XQ (2016); Effects of post-weld heat treatment on microstructure and mechanical properties of linear friction welded Ti2AlNb alloy, Mater. Des., 94, pp.45-53.

[4] Chen X, Xie FQ, Ma TJ, Li WY and Wu XQ (2016); Microstructural evolution and mechanical properties of linear friction welded Ti2AlNb joint during solution and aging treatment, Mater. Sci. Eng. A, 668, pp.125-136.

[5] Zhang K, Ni L, Lei Z, Chen Y and Hu X (2016); Microstructure and tensile properties of laser welded dissimilar Ti-22Al-27Nb and TA15 joints, Int. J. Adv. Manuf. Technol., pp.1-8.

[6] Lei Z, Dong Z, Chen Y, Zhang J and Zhu R (2013); Microstructure and tensile properties of laser beam welded Ti-22Al-27Nb alloys, Mater. Des., 46, pp.151-156.

[7] Lei ZL, Dong ZJ, Chen YB, Huang L and Zhu RC (2013); Microstructure and mechanical properties of laser welded Ti-22Al-27Nb/TC4 dissimilar alloys, Mater. Sci. Eng. A, 559, pp. 909-916.

[8] Tan LJ, Yao ZK, Ning YQ and Guo HZ (2011); Effect of isothermal deformation on micro-structure and properties of electron beam welded joint of Ti2AlNb/TC11, Mater. Sci. Technol., 27 (9), pp.1469-1474.

[9] Tan LJ, Yao ZK, Wang T and Guo HZ (2011); Effect of post-weld heat treatment on micro-structure and properties of electron beam welded joint of Ti2AlNb/TC11, Mater. Sci. Technol., 27 (8), pp.1315-1320.

[10] Li Y, Zhao Y, Li Q, Wu A, Zhu R and Wang G (2017); Effects of welding condition on weld shape and distortion in electron beam welded Ti2AlNb alloy joints, Mater. Des., 114, pp. 226-233.

[11] Yadaiah N, Bag S, Paul CP and Kukreja LM (2015); Fiber laser welding in a controlled inert gas atmosphere: An experimental and numerical investigation, in Laser Based Manufacturing, Springer, Chapter 20, pp.399-419.

[12] Yadaiah N, Bag S, Paul CP and Kukreja LM (2016); Influence of self-protective atmosphere in fiber laser welding of austenitic stainlesssteel, Int. J. Adv. Manuf. Technol., 86(1), pp. 853-870.

[13] Yadaiah N and Bag S (2014); Development of egg-configuration heat source model in numerical simulation of autogenous fusion welding process, Int. J. Ther. Sci., 86, pp. 125-138.

[14] Yadaiah N and Bag S (2013); Role of Oxygen as Surface-

Active Element in Linear GTA Welding Process, J. Mater. Eng. Perfor., 22(11), pp. 3199-3209.

[15] Yadaiah N and Bag S (2012); Effect of heat source parameters in thermal and mechanical analysis of linear GTA welding process, ISIJ Int., 52(11), pp. 2069-2075.

[16] Luo Y, You G, Ye H and Liu J (2010); Simulation on welding thermal effect of AZ61 magnesium alloy based on three-dimensional modeling of vacuum electron beam welding heat source, Vacuum, 84,pp. 890–895.

[17] Chiumentia M, Cervera M, Dialami N, Wu B, JinweiL and Saracibar CA (2016); Numerical modeling of the electron beam welding and its experimental validation, Finite Elem. Anal. Des., 121, pp.118–133.

[18] Lacki P and Adamus K (2011); Numerical simulation of the electron beam welding process, Comput. Struct., 89, pp. 977–985.

[19] Lacki P, Adamus K and Wieczorek P (2014); Theoretical and experimental analysis of thermo-mechanical phenomena during electron beam welding process, Comput. Mater. Sci., 94, pp. 17-26.

[20] Bardel D, Neliasa D, Robin V, Pirling T, Boulnat X and Perez M (2016); Residual stresses induced by electron beam welding in a 6061 aluminium alloy, J. Mater. Process. Technol., 235, pp.1-12.